Surface modifications of inert and bioactive glasses with plasma-deposited polymer coatings to impart antiadhesive properties

Surfaces and Interfaces 64 (2025) 106346

Contents lists available at ScienceDirect

Surfaces and Interfaces

journal homepage: www.sciencedirect.com/journal/surfaces-and-interfaces

Surface modifications of inert and bioactive glasses with plasma-deposited polymer coatings to impart antiadhesive properties

Marta Miola [a,b,*], Kevin Pontillo [a], Katiuscia Costabello [c], Manuel Lai [c], Sara Ferraris [a,b], Ziba Najmi [d], Andrea Cochis [d], Lia Rimondini [d], Enrica Vernè [a,b]

[a] Department of Applied Science and Technology, Politecnico di Torino, Institute of Materials Engineering and Physics, Corso Duca degli Abruzzi, 24 10129 Torino, Italy
[b] PolitoBioMED Lab, Politecnico di Torino, Corso Castelfidardo, 30A 10129 Torino, Italy
[c] IRIS S.r.l., Via Giovanni Paolo II, 26 10043 Orbassano TO, Italy
[d] Department of Health Sciences, Center for Translational Research on Autoimmune and Allergic Diseases-CAAD, Università del Piemonte Orientale UPO, Novara 28100, Italy

ARTICLE INFO

Keywords:
Bioactive glass
Inert glass
Non-thermal atmospheric plasma treatment
Antiadhesive

ABSTRACT

The development of antiadhesive surfaces has attracted great interest in recent years, both in the biomedical field and in everyday life applications. Non-thermal atmospheric plasma technology, still slightly explored in particular on bioactive glass, offers important opportunities for limiting bacterial adhesion on materials' surfaces. In this work, both bioactive and inert glasses were coated with (HMDSO) using the non-thermal atmospheric plasma process. The obtained coating was carefully investigated through morphological and compositional analysis, and the evaluation of the surface roughness wettability and zeta potential. Moreover, the influence of the coating on bioactivity (for bioactive glasses) was estimated and a preliminary test to investigate the antifouling properties of treated samples was performed using a Multi-Drug Resistant (MDR) *Staphylococcus aureus* strain. The obtained results evidenced a reduced roughness and a uniform distribution of the polymer on all glasses' surfaces, which imparted a hydrophobic effect due to the exposure of CH_3 groups. The bioactivity kinetics of the treated samples slightly decreased; however, the hydroxyapatite (HAp) precipitation was highlighted after 7 days of immersion in SBF. Finally, all plasma treated glasses showed a significant reduction in the number and aggregation degree of viable surface-adhered MDR *S. aureus*.

1. Introduction

The ongoing advancements in materials research have fostered a growing interest in enhancing the performance of glass across various sectors, ranging from biomedical applications to construction. Considering recent developments, antibacterial activity has emerged as a crucial property for reducing the spread of infectious diseases [1–4]. To achieve this objective, it is possible to modify the surface of these materials both morphologically and chemically. Thus, it is essential to tailor the glass surface with methods that ensure stable and long-lasting antimicrobial properties under varying conditions of use and over extended periods, without compromising the optical and mechanical properties of the bulk material.

Antibacterial coatings on window glass hold promise for healthcare infrastructures, effectively preventing surfaces from serving as vectors for pathogens [5,6]. In the field of bone regenerative medicine, the antimicrobial surfaces of bioactive glasses can be leveraged to inhibit post-implantation infections, thereby promoting tissue growth and osteointegration [7].

Antibacterial properties can be imparted to materials through various approaches, such as incorporating chemical agents onto the material's surface through different types of interactions (e.g., electrostatic attraction, covalent and hydrogen bonds) or modifying surface morphology and topography [8–10]. The antimicrobial action can manifest in diverse ways: functionalized surfaces can prevent the adhesion of pathogenic bacteria, inhibit their proliferation, or induce bacterial death [11].

Promising techniques for surface modification of materials include plasma treatments, which can alter the substrate's roughness and patterning while facilitating the grafting of functional groups [12].

* Corresponding author: Politecnico di Torino, Department of Applied Science and Technology, Institute of Materials Engineering and Physics, Corso Duca degli Abruzzi, 24 10129, TORINO, ITALY.
E-mail address: marta.miola@polito.it (M. Miola).

https://doi.org/10.1016/j.surfin.2025.106346
Received 16 September 2024; Received in revised form 20 February 2025; Accepted 27 March 2025
Available online 28 March 2025

These groups are critical for reducing surface free energy and, consequently, enhancing hydrophobicity, which is crucial for anti-biofouling functions [13,14].

Different strategies have been also investigated to impart antimicrobial properties to glass surfaces. Concerning bioactive glasses, their surface can be enriched with antimicrobial elements (e.g. Ag, Cu, Zn) [15,16] or nanoparticles [17,18]. For example, Vernè and co-workers design a simple and efficient method by ion-exchange technique in an aqueous solution to introduce silver and copper to different bioactive glass compositions [19]. The same research group has also investigated various physical and chemical processes, especially the use of polyphenols, to reduce Ag or Cu nanoparticles in situ on the surface of bioactive glasses [20]. The nucleation of Ag nanoparticles on the surface of a bioactive glass has been also induced by a sonochemical method followed by a thermal treatment by Gonzalo-Juan et al. [21]. Antimicrobial properties can be also imparted by functionalizing the glass surfaces with antibacterial drugs or biomolecules [22,23], such as lysozyme or antibiotics. Moreover, the development of anti-adhesive surfaces has also been explored; for example, Shaikh et al. used a femtosecond laser to tailor the surface roughness, wettability and surface chemical composition to limit the bacterial attachment and biofilm formation on the 45S5 Bioglass® [24].

The performance of antimicrobial coatings is also relevant on multipurpose glass surfaces. For instance, Won et al. assessed the feasibility of transparent TiO_2 films to confer antibacterial properties to commercially available products [25]. Choi and colleagues investigated zinc aluminate as an environmentally friendly coating material for smartphone panel glasses, showing strong antibacterial activity against *Escherichia coli* and S. aureus [26]. The efficacy of UV irradiation-driven antimicrobic activity of commercial glass SaniTiseTM was determined by Kisand et al., who assumed that bactericidal properties relied on the degradation of the cell wall due to the production of reactive oxygen species during the photocatalytic process of TiO_2 [3]. Other authors investigated the functionalization process to impart antibacterial action to glasses; for example, Gkana et al., verified the antiadhesive properties of glasses coated with two different commercial nanoparticle compounds based on organo-functionalized silanes [27], evidencing an anti-adhesion and anti-biofilm effect of the organosilane based products. Marra and co-authors propose an antibiofilm coating based on hybrid nanoparticles (TiO_2, ZnO_2)-melanin agents functionalization on glass surface previously treated with oxygen cold plasma [28], highlighting the efficacy of the coated glasses, especially for melanin-TiO_2 functionalized glass, to prevent biofilm formation. Glasses with an antibacterial action are also currently marketed by Corning® (Antimicrobial Corning Gorilla® Glass) and AGC glass, introducing silver ions onto the surface of the glasses [29,30].

As previously mentioned, the use of plasma to confer antibacterial/anti-adhesive properties has also been investigated in the literature, although in the field of biomaterials mainly on metal and polymeric surfaces. Plasma technology can be used for surface activation, coating deposition or surface nanostructuring. This technology, in particular non-thermal atmospheric pressure plasma, has numerous advantages compared to processes currently used or investigated, such as the possibility of modulating the surface of materials from the micro-nano to the molecular/atomic scale. Plasma treatment is also a dry process with limited energy costs and low environmental impact [31].

The use of plasma to impart antibacterial properties to glasses (both inert glass and bioactive glass) is still little explored. Some authors report the use of plasma to pretreat the surface of the glass, subsequently functionalized with different antimicrobial agents (e.g. antimicrobial peptides, silver or quaternary ammonium salt) [32–34]. Other studies have investigated the possibility of directly depositing antibacterial agents via plasma, increasing the hydrophobicity and thus the bacteria adhesion or creating nanostructured surfaces with antimicrobial action [35–38], using different substrates including glasses.

This work aimed to use the non-thermal atmospheric pressure plasma technology to activate and coat with hexamethyldisiloxane (HDMSO) an inert glass (for fenestration) and two bioactive glass (SBA2 and S53P4 [39,40]) to impart them antiadhesive effect, comparing the obtained properties. According to the authors' knowledge, the use of plasma technology to confer antibacterial or antiadhesive properties is still little explored in the field of bioactive glasses and ceramics. However, this approach could represent a valid and efficient alternative to antimicrobial chemical agents and drugs, since it is also effective against multi-resistant strains. The plasma deposition was verified through morphological-compositional analyses and the investigation of surface wettability and charge. The antiadhesive effect against Staphylococcus aureus was also assessed together with, for bioactive glasses, the possible influence on bioactivity.

2. Materials and methods

2.1. Samples preparations

In this work, two bioactive glass compositions: i) a commercial one (S53P4, commercially know as BonAlive®: 53 % SiO_2, 23 % Na_2O, 20 % CaO, 4 % P_2O_5, wt %), ii) a composition previously designed by the authors (SBA2: 48 % SiO_2, 18 % Na_2O, 30 % CaO, 3 % P_2O_5, 0.43 % B_2O_3, 0.57 % Al_2O_3, mol %) [41–43], and an inert soda-lime glass for windows (supplied by IRIS S.r.l) were used. The SBA2 and S53P4 bioactive glasses were synthesized by melting the reactants at 1450 °C for 1 h and 1360 °C for 3 h respectively (Nabertherm® LHT 04/18, Germany), quenching the melt in a cylindrical brass mould and annealing the SBA2 at 500 °C for 13 h and S53P4 at 500 °C for 1 h. Subsequently, the obtained bars were cut in slices of 10 mm in diameter and 7 mm in height using an automatic cutting machine (ATM® Brillant 220), which were polished with SiC abrasive papers ranging from 800 to 4000 grids to level the surfaces using an automatic polishing machine (Struers® LaboPol-2) at 500 rpm according to following protocol: roughing at P600, progressive polishing at P800 for 30 s, P1000 for 60 s, P1200 for 90 s, P2500 for 120 s and P4000 for 150s. The inert soda-lime glass was provided in 20 × 20 × 4 mm; in order to compare the bioactive and bioactive glasses, some window glass samples were subjected to the same polishing process of SBA2 and S53P4.

2.2. Plasma treatment

The 4 types of glasses (SBA2, S53P4, soda-lime glass and polished soda-lime glass) were subjected to an atmospheric plasma treatment, using a reactor in dielectric barrier discharge (DBD) configuration by IRIS S.r.l. All samples were pretreated in He and O_2, to enhance the exposure of surface hydroxyl groups, useful for monomer grafting. Subsequently, they were coated with HMDSO, in order to confer hydrophobic properties to the surface. Table 1 resumes the plasma treatment conditions and Table 2 the acronyms of different samples.

For both the pretreatment and the coating deposition a voltage of 6 kV and a frequency of 5 kHz were used. The samples were placed in the gap between the two plates of the reactor and the plasma was applied for 45 s in the case of pretreatment and for 90 s for the deposition of HMDSO.

2.3. Samples characterization

2.3.1. Morphological and compositional characterization

Morphological and compositional investigations of the glasses' surface were carried out by field emission scanning electron microscopy (FESEM, SUPRATM 40, Zeiss) equipped with energy dispersive X-ray spectroscopy (EDS). Samples were coated with a thin Pt layer before the analysis.

Attenuated Total Reflection Fourier Transform IR (ATR-FTIR) spectroscopy (Nicolet iS50 FTIR Spectrometer) was used to investigate the surface chemistry of samples and the deposition of HMDSO. The spectra

Table 1
Pretreatment conditions and plasma coating.

		Gas flow (l/min)			Plasma parameters		
		He	O_2	HMDSO in He	Voltage (kV)	Frequency (kHz)	Time (s)
Plasma treatment	Pretreatment	8	0.2	–	6	5	45
	Coating	8	–	0.4	6	5	90

Table 2
Samples preparations and acronyms.

Samples	Polishing	HMDSO Plasma treatment
SBA2	Yes	No
SBA2_T	Yes	Yes
S53P4	Yes	No
S53P4_T	Yes	Yes
W	No	No
W_T	No	Yes
W_P	Yes	No
W_P_T	Yes	Yes

were acquired in the range 400–4000 cm^{-1} with a resolution of 4 cm^{-1} with 32 scansions for each spectrum. OPUS software (v. 6.5, Bruker S.p. A) was used for instrumental control and spectral acquisition.

2.3.2. Surface properties characterization

The topographical features of the glasses were investigated with a laser optical profilometer (LSM 900, ZEISS, Germany), wettability (Krüss DSA 100, Germany) and surface energy measurements. The surface roughness parameters, in particular Sq, were obtained using a laser optical profilometer with a 20x objective, using the Confomap software.

The surface wettability was analysed with a static contact angle, using the sessile drop technique and water (WCA). Three measurements were performed for two glasses of each type, and the contact angle was automatically measured after 2 s for each tested sample. Results are reported as average ± standard deviation (SD). Statistical analysis was performed using one sample Student *t*-test. P values < 0.05 were considered significant.

The zeta potential in function of pH of bioactive glasses and the inert polished soda-lime glass, before and after plasma treatment, were also analysed using an electrokinetic analyzer (SurPASS, Anton Paar) equipped with an adjustable gap cell and an automatic titration unit. KCl 0.001 M was used as electrolyte, NaOH and HCl 0.05 M as titration solutions for the basic and acidic range respectively. For each pH point, 4 measurements were performed and reported as mean and standard deviation on the titration curve. A different set of samples was used for acidic and basic titration to avoid effects due to sample reaction during the measurement.

The adhesion properties of the coating were evaluated by means of a semi-quantitative analysis, the cross-cut tape test, according to the standard ASTM D 3359–97 ("Standard test methods for measuring adhesion by tape test"). Due to the size of the samples, the analysis was carried out only on polished fenestration glass. Subsequently, the samples were subjected to a confocal microscope and FESEM observation, and an FTIR analysis was performed to detect the presence of the coating.

2.3.3. In vitro bioactivity test

The ability of bioactive glasses to induce the precipitation of HAp after plasma treatment was investigated by dipping SBA2 and S53P4 in 50 mL of simulated body fluid (SBF – Kokubo protocol [44]) maintained at 37 °C for 3, 7 and 14 days.

At the end of each incubation time, the pH of the solution was monitored and samples were removed from SBF solution, rinsed in bi-distilled water and dried at room temperature. Afterwards, samples were analysed by means of FESEM-EDS to verified the HAp presence.

2.4. In vitro antiadhesive activity evaluation

2.4.1. Bacterial culture medium and conditions of growth

To evaluate the impact of plasma treatment on the adhesion behaviour of bacteria on the inert (soda-lime and polished soda-lime) and bioactive (S53P4 and SBA2) glasses, a preliminary evaluation was carried out using gram-positive Multi-Drug Resistant *Staphylococcus aureus* (MDR *S. aureus*). This bacterial strain was purchased from the American Type Culture Collection (ATCC; ATCC 43,300; Manassas, Virginia, USA) and is considered a main cause of infections associated with orthopaedic implants [45].

Bacteria were cultivated on Trypticase Soy Agar (TSA, Merck, Milan, Italy) and incubated at 37 °C for 24 h to allow single bacterial colonies to grow. Subsequently, a few colonies were collected and diluted into 20 mL of Luria Bertani broth (LB, Merck, Milan, Italy). Broth cultures were incubated overnight at 37 °C under agitation (120 rpm in an orbital shaker). A fresh broth sub-culture was prepared before each experiment to test bacteria in their exponential growth phase. Accordingly, the bacteria concentration was further diluted into fresh LB broth to a final concentration of 1×10^5 cells/mL, corresponding to an optical density (OD) of 0.001 at wavelength 600 nm, determined by a spectrophotometer (Spark, Tecan, Switzerland). Fresh LB medium was used as a blank to normalize the OD values.

2.4.2. Antifouling activity evaluation

Prior to biological assays, the samples were sterilized with UV-C light for 30 min on each side. To evaluate the antifouling properties of non-treated and plasma-treated samples, the International Organization for Standardization protocol (ISO; ISO 22196) was utilized. This protocol is designed to analyse the antifouling behaviour of samples' surfaces by directly infecting them with a bacterial suspension [42]. Accordingly, the sterile samples were placed into suitable multiwell plates based on their dimensions (24-multiwell and 6-multiwell plates for bioactive glasses with diameter 10 mm and inert glasses with a size 20 × 20 cm, respectively). A certain volume of the bacterial suspension (50 μL for bioactive glasses and 500 μL for inert glasses) containing 1×10^5 CFU/mL, was directly dropped onto the specimens' surfaces and covered with sterile polyethylene film. The inoculated specimens were placed in an incubator at 37 °C for 90 min to allow the bacterial cells to attach to the surfaces of the samples [46]. At this time point, each sample was washed with sterile phosphate-buffered solution (PBS) to remove non-adhered bacterial cells from the surfaces. The viable surface-adhered bacterial colonies were then counted the using colony forming unit (CFU) method. Briefly, surface-adhered bacteria were detached using sonication (5 min, 3 times), and vortex (30 s, 3 times), followed by performing six serial 10-fold dilutions by mixing 20 μL of bacteria with 180 μL of PBS as previously described by the Authors [16, 47]. The total CFU count was determined using the following formula:

$$\mathrm{CFU} = \left[\left(\mathrm{numberofcolonies} \times \mathrm{dilutionfactor} \right)^{\wedge(\mathrm{serialdilution})} \right]$$

The formation of bacterial microcolonies or biofilm layers on the surfaces was visually assessed using Scanning Electron Microscopy (SEM, JSM-IT500, JEOL, Tokyo, Japan) images. The specimens were dehydrated using an ethanol gradient (70 %, 90 % ethanol for 1 h each and 100 % ethanol for 2 h), rapidly dried with hexamethyldisilazane, and coated with a gold layer using the JEOL Smart Coater (JEOL, Japan). Images were collected at different magnifications (× 2000 and × 4000)

using a secondary electron detector.

For evaluation of the thickness and distribution of bacterial aggregations (microcolonies), and for the calculation of the occupied surface area on the samples' surfaces by bacterial strains, two software programs were utilized: SMILE VIEW™ map (version 8.2.9621, JEOL) and image processing software (ImageJ). For both software programs, SEM images at low magnifications (× 2000) were used and noise from the background was removed by setting thresholds for minimum and maximum values. Subsequently, the 3D image was automatically reconstructed by SMILE VIEW software, providing information about the thickness, height, and distribution of bacteria, which were shown as peaks. In ImageJ software, bacterial cells were automatically counted, and the occupied surface areas on the samples' surfaces by bacterial cells were calculated.

2.4.3. Statistical analysis

All biological experiments were performed in triplicate. The statistical analysis of the data was carried out by SPSS software (v.20.0, IBM, USA). Initially, the normal distribution of the data and the homogeneity of variance were assessed by the Shapiro-Wilk's test and Levene's test, respectively. Then, the results of the treated groups were compared with the control ones by one-way comparison ANOVA and Tukey's test as a post hoc analysis. P value < 0.05, and p value < 0.01 were considered as statistical differences shown here by * and **, respectively.

3. Results and discussions

3.1. Morphological and compositional characterization

FESEM analyses were performed in order to highlight the presence of the polymer coating. The obtained images (Figs. 1 and 2) show the presence of spherical particles on all samples treated with plasma, ascribable to the polymer deposition, as observed also by Stallardand co-authors [48]. In particular, SBA2_T glass displays spheres with two orders of magnitude, micrometric (evidenced with arrows in Fig. 1d) and submicrometric dimensions (Fig. 1e), mainly arranged following the pattern of parallel lines generated by the polishing process. The S53P4 glass also presents a preferential orientation of the spheres in the direction of the polishing lines, but in this case, the spheres have more uniform dimensions, of a few hundred nm (Fig. 1k, l).

Concerning the window glasses (Fig. 2), a partial orientation of the spheres along the polishing lines is observable for the W_P_T sample (Fig. 2k, l); while for W_T glass, the spherical particles are distributed according to a random pattern (Fig. 2d, e). W_P_T glass shows a coating formed by spheres with larger dimensions than that of the unpolished samples (W_T), in which particles of a few tens of nm are significantly distinguishable. However, for all the treated samples, a clear difference in morphology is observed compared to the respective untreated samples, which, together with the other analyses, highlights the effective

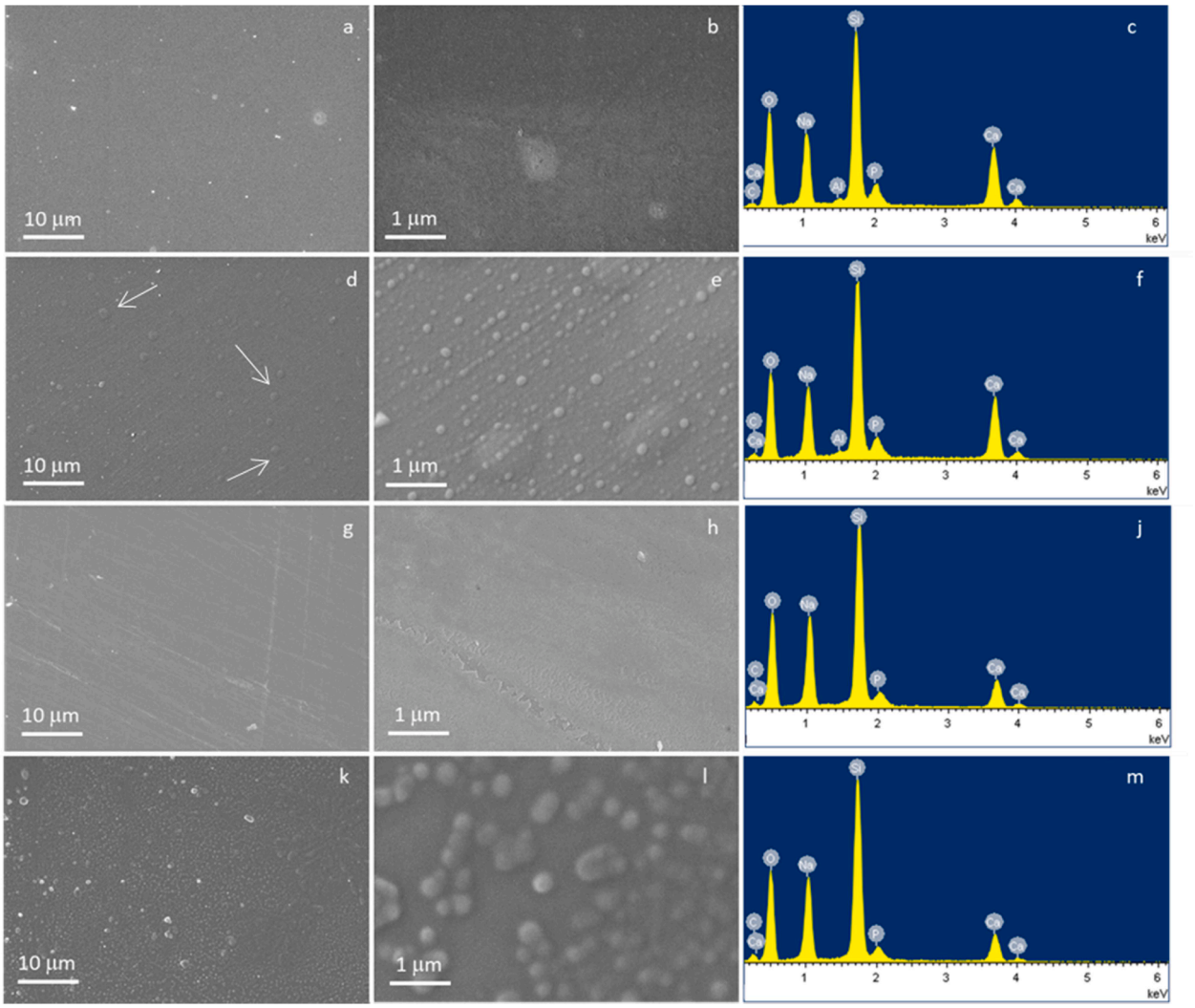

Fig. 1. FESEM-EDS analysis of a), b) and c) SBA2, d), e) and f) SBA2_T, g), h) and j) S53P4, k), l) and m) S53P4_T. a), d), g) and k) magnification 5kx, b), e), h) and l) magnification 50kx.

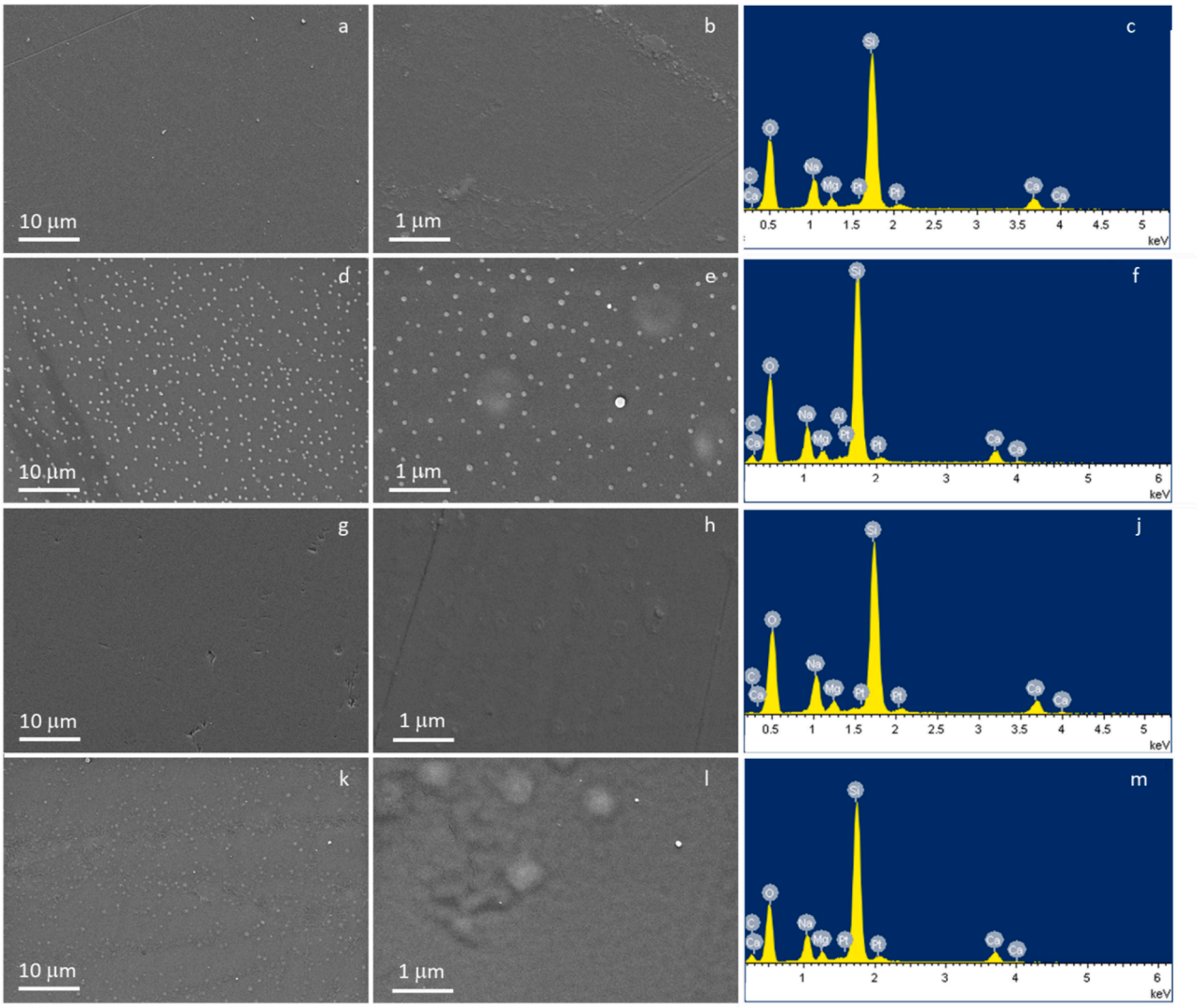

Fig. 2. FESEM-EDS analysis of a), b) and c) W, d), e) and f) W_T, g), h) and j) W_P, k), l) and m) W_P_T. a), d), g) and k) magnification 5kx, b), e), h) and l) magnification 50kx.

deposition of the polymer.

The compositional analysis, performed on plasma-treated (Fig. 1c,f,j, m) and untreated glasses (Fig. 2c,f,j,m), revealed a significant increase (t student, $p = 0.017$ for polished window glass) in the carbon amount for plasma-treated glasses, attributable to the deposited polymer. The C increase was most consistently observed in window glasses (with an increase of over 200 % in %at) with respect to bioactive ones, since bioactive glasses, more reactive than window glasses, can be subjected to carbonation phenomena on their surface. The other elements have not undergone significant changes.

3.2. Surface properties characterization

The polymer presence was verified through FTIR analysis (Fig. 3). All glasses showed the peaks (highlighted with a blue dotted line in Fig. 3a) at about 750 cm^{-1} and the band at 1000–1200 cm^{-1} ascribable respectively to the Si-O symmetric stretching and the asymmetric stretching of Si-O-Si bonds, together with a band at 850 and 950 cm^{-1} related to SiO_4 tetrahedron structures containing non-bridging oxygen [49,50]. Moreover, the plasma-treated glasses displayed the characteristic peaks of the HMDSO (evidenced with a black dotted line in the Fig. 3b) demonstrating the effective deposition of the polymer: at about 3000 cm^{-1} a peak due to the asymmetric stretching of the methyl group in Si-CH_3 is observed, and the peak at about 1260 cm^{-1} can be ascribed to the bending of CH_3, while the band at about 1400–1350 cm^{-1} can be attributed to the asymmetric deformation vibration of CH_3 groups. Around 800 cm^{-1} an enlargement of the peak concerning the Si-O symmetric stretching can be noticed, probably caused by its convolution with the peaks regarding the rocking of -CH_3 and the stretching of Si-C in the bond Si-CH_3 [51–53]. Some peaks of HMDSO, in particular those at 1071 and 1015 cm^{-1}, ascribable to Si–O–Si and Si–O–C, are not visible because they overlap with that of the glass. The enlargements reported in Fig. 3 highlight the main peaks of the polymer found on the treated samples.

As reported by some authors, using noble gases in HMDSO plasma deposition the molecule is fragmented in two main film-forming species: (CH_3)x-Si-O· and (CH_3)x-Si· by scission of a Si–O bond [54,55]. Depending on the bond that the molecule makes with the OH groups of the glass, different functional groups can be exposed [54]. However, the analyses conducted in this paper allow us to mainly note the presence of CH_3 groups which impart a hydrophobic character to the treated glasses

Since in addition to wettability, roughness can also have a role in bacterial adhesion, the roughness values were estimated using the laser optical profilometer; the obtained results are reported in Fig. 4. Concerning the untreated glasses, it was observed a higher Sq value for polished inert glass (W_P), due to the polishing treatment carried out on

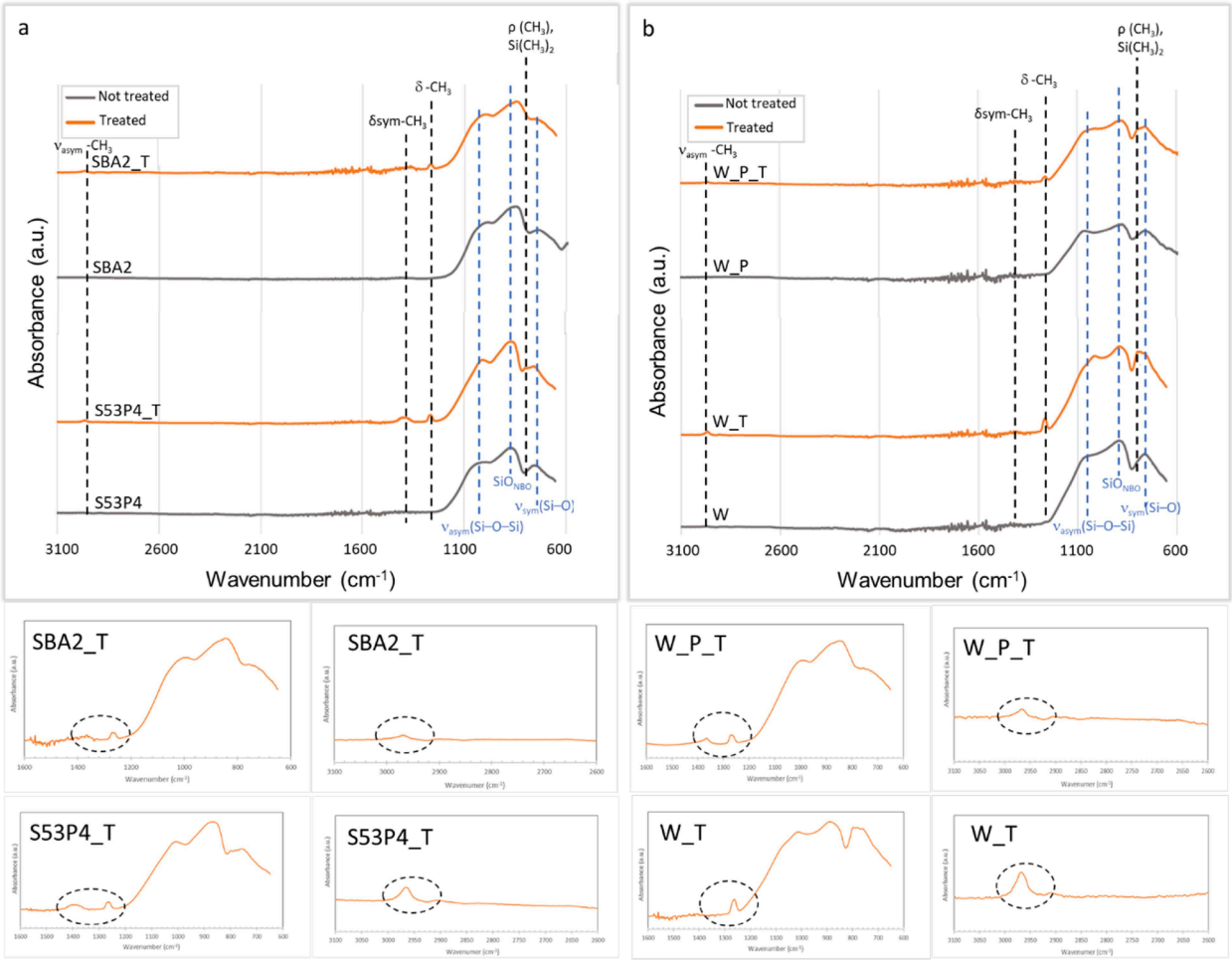

Fig. 3. FTIR analysis of a) bioactive glasses SBA2 and S53P4, b) inert window glasses. Complete spectrum at the top, expansion of the most significant peaks of HMDSO at the bottom.

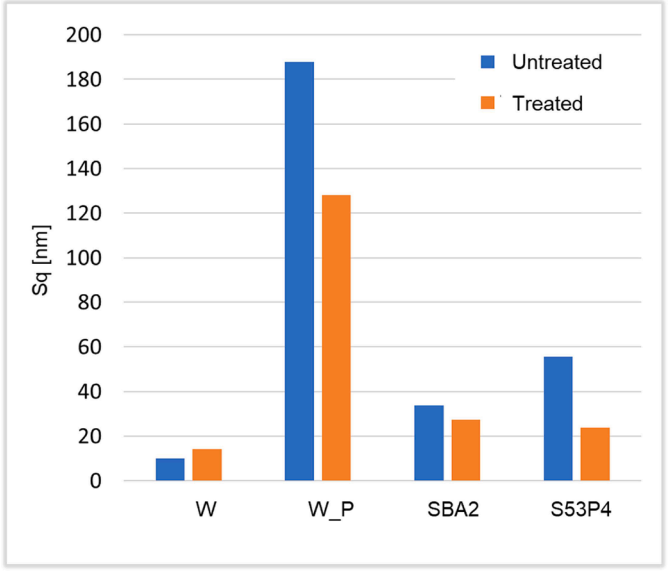

Fig. 4. Roughness values (Sq) for untreated and treated inert (W and W_P) and bioactive (SBA2 and S53P4) glasses.

the very smooth surface of the float glass, compared to the Sq values obtained for the other glasses subjected to polishing, SBA2 and S53P4. As expected, inert glass (W) showed the lowest Sq value. The HMDSO coating seems to reduce the roughness of all the polished samples, more significantly for the samples that present a higher roughness (W_P and S53P4), acting as a levelling film. However, this Sq decrease is not observed for the inert unpolished glass (W), for which a slight increase in roughness is noted, as evidenced also in other works in which the HMDSO was deposited on extremely flat surfaces [48,56].

Fig. 5 displays the values obtained by measuring the static contact angle of untreated and treated samples. A significant difference (t student, $p < 0.05$) in WCA between untreated W and W_P inert glasses can be observed. This discrepancy, according to wettability models [57,58], is ascribable to the roughness of the surface: the unpolished W glass has a smooth surface compared to the polished one (as demonstrated in Fig. 4) and thus shows a more hydrophobic behaviour. After the plasma treatment, a significant increase in WCA was observed for all the samples (t student, $p < 0.05$). In particular, the greatest difference in terms of WCA before and after the treatment is observed for S53P4 glass; however, the coating with HMDSO imparted a hydrophobic effect to all the investigated glasses, thanks to the exposure of CH_3 groups as highlighted by FTIR analysis [51,59]. The obtained contact angle can limit bacteria adhesion while maintaining cells colonization, balancing the anti-adhesive properties and cellular adhesion.

To evaluate the surface properties of the treated glasses, a zeta potential analysis was finally performed. Fig. 6 reports zeta potential titration curves of bare and treated glasses. The isoelectric point (IEP) of

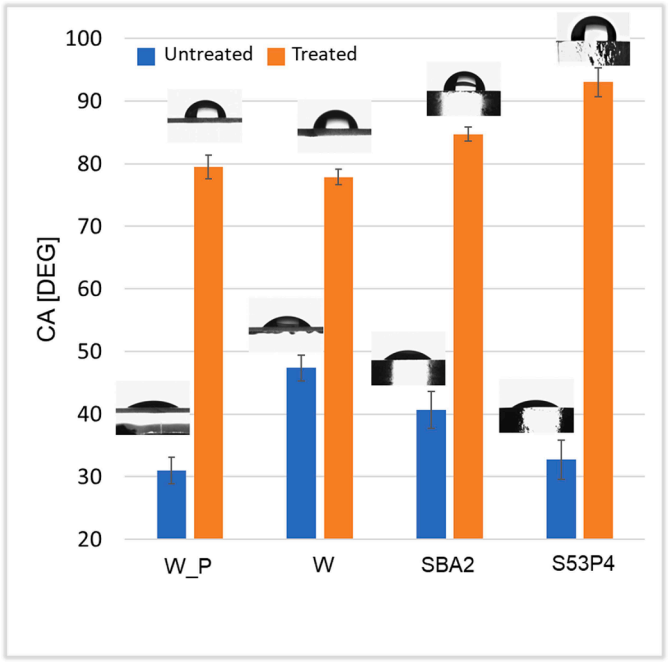

Fig. 5. static contact angle measurements.

bare glasses is acidic. In particular, IEP is lower than 3 for W_P and for S53P4 in accordance with reported values for silica and silica-based glasses [60,61] and previous measurements from the authors [62], and equal to 3.29 for SBA2, in accordance with previous work from the authors [63] and with the effect of oxides on the isoelectric point of silica-based glasses [61]. The acidic IEP is due to the presence of acidic functional groups (OH groups of silica-based glasses). Looking at the titration curve increasing acidity can be ascribed to OH groups of W, SBA2, and S53P4, due to the decreasing pH of the onset of the basic plateau (7, 6, 5.5 respectively), which represents the pH at which all OH groups are deprotonated.

After the treatment, an increase of the value of the IEP can be noticed. In particular, it can be observed that values move to 4.02, 3.29, and 3.19 for W_P_T, SBA2_T and S53P4_T respectively. All the values move close to pH 4, typical of inert polymers [64]. The effect seems more evident on the most inert glass (W), followed by SBA2 and S53P4. Moreover, the basic plateau is almost absent after the treatment, as a confirmation that the acidic OH groups are no longer prevalent on the surface due to the bond with the HMDSO.

Therefore, the surface characterizations evidenced the effective deposition of the polymeric coating, bonded with the surface of the glasses and the achievement of hydrophobic surfaces due to the exposure of the CH_3 groups. However, to estimate the adhesion of the coating, a tape test was performed on W_P_T samples. The window samples were used both for their useful dimensions and because the adhesion of the coating must be significant, particularly for these applications. Concerning bioactive glasses, as can be seen from the performed analyses in SBF solution, during the bioactivity process the coating is replaced with a layer of hydroxyapatite. Fig. 7 displays the FTIR analysis, the images acquired at confocal microscope and at FESEM after the tape test. FTIR spectrum (Fig. 7a) evidences the peak ascribable to the polymer coating (highlighted in the figure with dotted circles), already discussed in Fig. 3. The images reported in Fig. 7b,c and d show the presence of the coating, demonstrating an optimal adhesion of the coating to the substrate, since no damage can be noticed.

3.3. *In vitro bioactivity test*

Fig. 8 shows the FESEM-EDS analysis of bioactive glass SBA2 plasma-treated and untreated subjected to SBF immersion for up to 14 days. Concerning the SBA2 glass, a thick layer of silica gel is clearly visible after 3 days of immersion in SBF (Fig. 8a) together with the precipitation of the first hydroxyapatite (HAp) nuclei (Fig. 8b). The crystallization of HAp increases as SBF treatment continues for up to 14 days (Fig. 8c-f). The EDS analysis (Fig. 8 g) evidences a significant increase of Ca and P after 3 days and a decrease of Na and Si, confirming the formation of a Ca- and P-rich phase on a glass surface, with an atomic Ca/P ratio very close to HAp one (1.6). The plasma treatment causes a slight delay in the precipitation of HAp, as can be observed from the images in Fig. 8h-l and the graph relating to the EDS analysis (Fig. 8p). However, after 7 days of

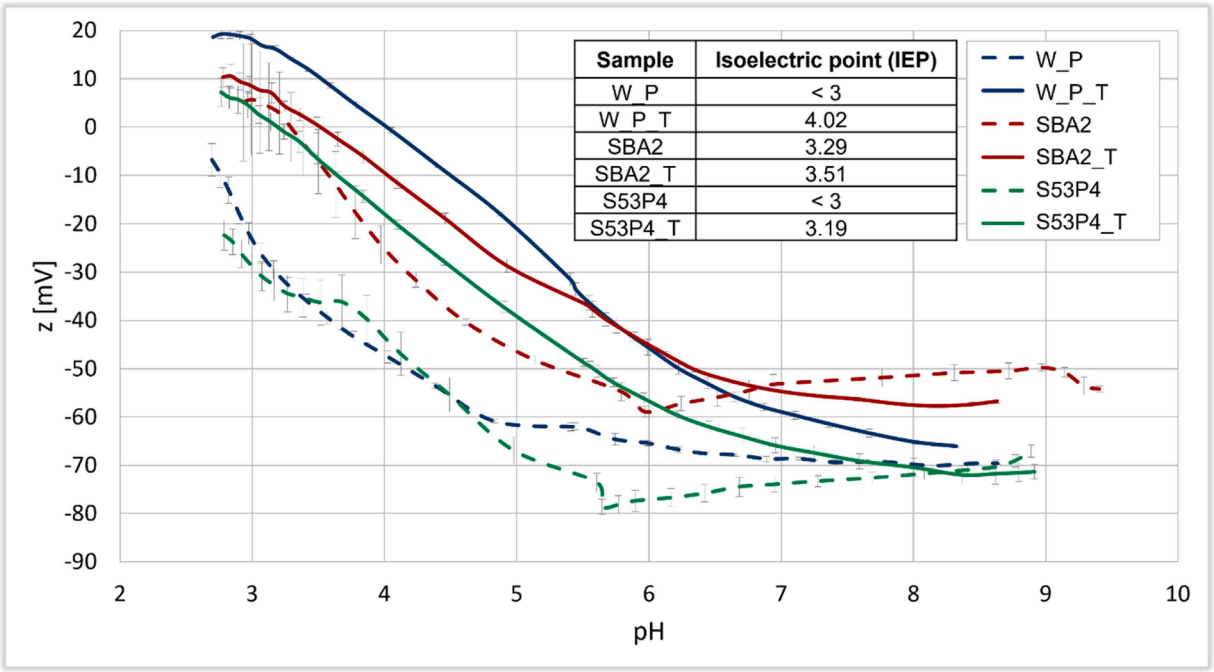

Fig. 6. Zeta potential titration curves of bare and treated glasses.

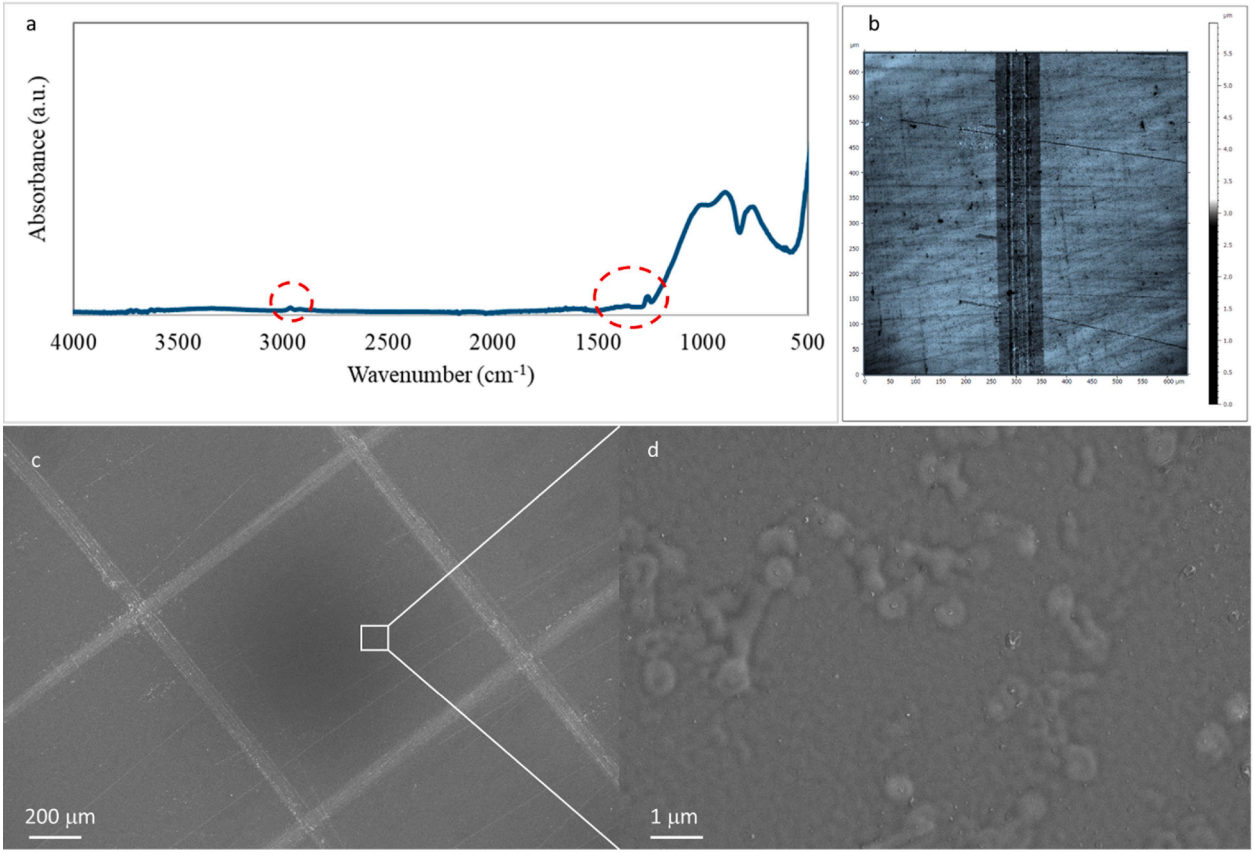

Fig. 7. a) FTIR spectrum, b) confocal microscope,c) and d) FESEM images of W_P_T samples after tape test.

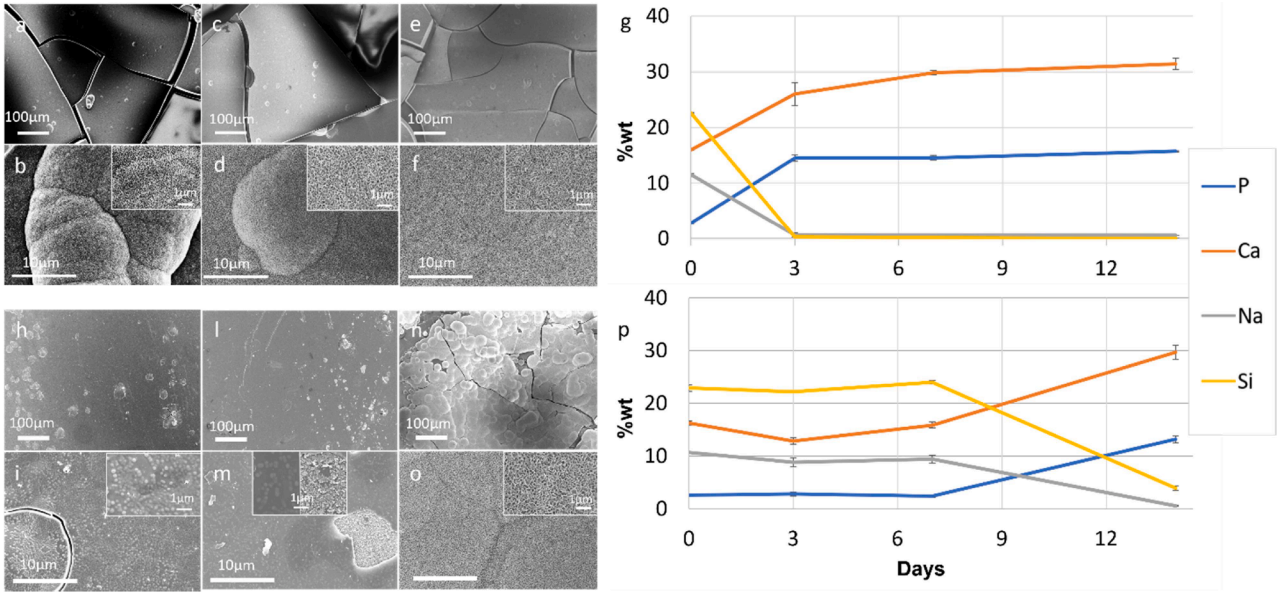

Fig. 8. FESEM micrographs of SBA2 immersed in SBF for a) and b) 3 days, c) and d) 7 days, e) and f) 14 days, and g) EDS analysis. FESEM micrographs of SBA2_T immersed in SBF for h) and i) 3 days, l) and m) 7 days, n) and o) 14 days, and p) EDS analysis.

SBF immersion, some precipitates with the typical morphology of *in vitro*-grown HAp can be detected on SBA2_T surface (Fig. 8m) and HAp formation becomes more substantial after 14 days (Fig. 8n, o). The Ca/P atomic ratio assessed by EDS results is1.7.

Regarding S53P4 glass, also in this case a slight delay in bioactivity kinetics was observed. Indeed, a thick layer of silica gel can be observed after 3 days of immersion in SBF on the untreated glass together with the first HAp nuclei (Fig. 9a, b). The HAp precipitation consolidates after 7 and 14 days (Fig. 9c-f).

On S53P4_T samples, however, the formation of silica gel and HAp is noticeable starting from 7 days of SBF immersion (Fig. 9l, m). The bioactivity kinetics are also confirmed by the EDS data (Fig. 9 g, p),

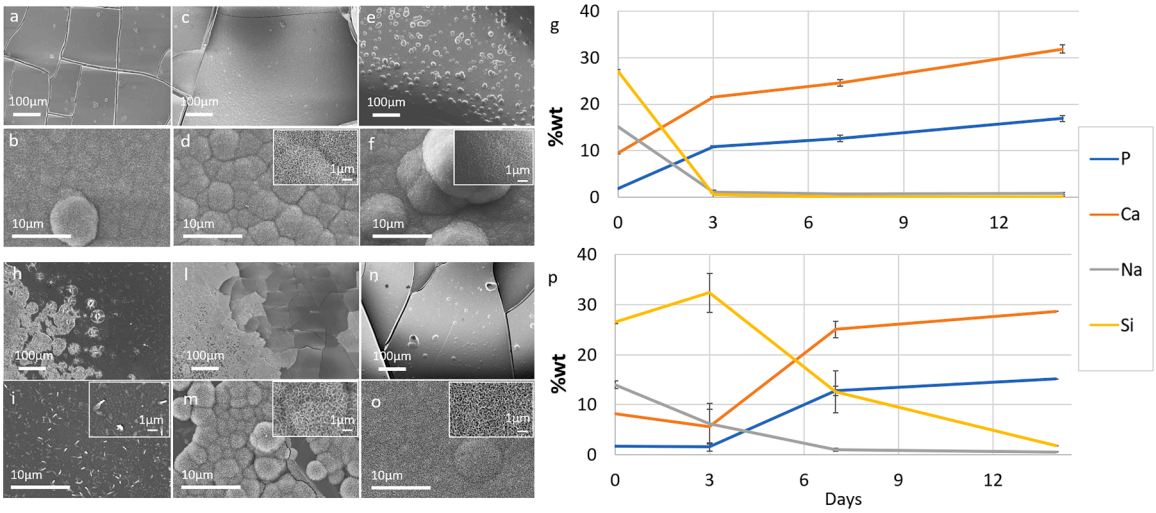

Fig. 9. FESEM micrographs of S53P4 immersed in SBF for a) and b) 3 days, c) and d) 7 days, e) and f) 14 days, and g) EDS analysis. FESEM micrographs of S53P4_T immersed in SBF for h) and i) 3 days, l) and m) 7 days, n) and o) 14 days, and p) EDS analysis.

which highlight an increase of Ca and P content and a decrease of Si and Na already after 3 days for S53P4, while these trends are observable for S53P4_T after 7 days. Both samples show a Ca/P ratio after 14 days of immersion of 1.5, thus showing the Ca-deficient nature of the formed hydroxyapatite.

In conclusion, the obtained results highlight a slight delay in the nucleation kinetics of hydroxyapatite for all plasma treated samples. In any case, the presence of the coating does not inhibit the bioactivity of the treated samples which are therefore potentially able of establishing *in vivo* a chemical bond with the bone tissue.

3.4. Antifouling activity evaluation

To evaluate the *in vitro* antifouling properties of the HDMSO plasma–treated inert glasses (W and W_P) and bioactive glasses (S53P4 and SBA2), the gram-positive, multidrug-resistant bacterial pathogen MDR *S. aureus* was chosen. This bacterium represents up to two-thirds of all pathogens involved in orthopaedic implant–related infections [65]. Since the treatment of *S. aureus* infections is complicated due to its multidrug–resistant behaviour, preparing samples with intrinsic antifouling characteristics to mitigate bacterial adherence (the first stage of pathogenicity) is promising [66].

The antifouling properties of the HDMSO plasma–treated samples were compared to those of the corresponding untreated samples. Based on the ISO 22,196 protocol, the samples' surfaces were directly infected with bacterial suspensions at a concentration of 1×10^5 CFU/mL. After 90 min of incubation and the removal of non-adhering bacterial cells by washing with PBS, the number of viable bacterial colonies and the morphology of bacterial aggregations on the samples' surfaces were analysed using CFU counts and SEM images, respectively.

The results are presented in Figs. 10 and 11. Since the 90 min incubation period is dedicated to the attachment of bacteria to the surfaces, not for growth, and the removal of non-adhered bacteria during the washing step, the untreated samples showed a smaller number of surface–attached bacterial colonies than the starting number, which was 1×10^5 CFU/mL (indicated by the red line in Fig. 10a). However, significantly fewer bacterial cells adhered to the treated samples' surfaces (both inert and bioactive glasses), and a statistically significant difference was observed between HDMSO-treated and untreated samples (Fig. 9a, p values < 0.01 and < 0.05, indicated with ** and *, respectively). CFU counts did not detect any growth of bacterial colonies on the surfaces of HDMSO plasma–treated W_P and S53P4 samples, which was also shown in the CFU agar plate images (Fig. 10b). Additionally, a statistically significant reduction in the number of adhered bacteria on the surfaces of treated W and SBA2, approximately 2 Log and 1 Log respectively, was observed compared to the untreated W and SBA2 as their control samples (Fig. 10a,b; p value < 0.05 indicated by *). SEM images captured from the surfaces of the untreated and treated samples (W, W_P, S53P4, and SBA2) confirmed the results obtained from CFU counting. As shown in Fig. 10c, some bacterial aggregations and microcolonies formed on the untreated samples, especially on the surfaces of W_P, S53P4, and SBA2, while only a few single colonies adhered to the surfaces of all treated samples, with no bacterial aggregations observed.

Checking the thickness of bacterial aggregations in the 3D-reconstructed SEM images (Fig. 10d) demonstrated the presence of aggregations with heights between 2–5 μm for the untreated W_P, S53P4, and SBA2. For example, the thickness of aggregations on the untreated S53P4 was mostly between 2–4 μm, with some microcolonies reaching higher heights (5–8 μm). As expected, not only were no bacterial aggregations or microcolonies detected in the 3D-reconstructed SEM images of treated samples, but the height of bacterial cells was mostly between 1–2 μm, which, according to the dimension of *S. aureus,* corresponds to single colonies (Fig. 10d).

Calculation of the occupied surface area on the samples' surfaces by bacterial cells using ImageJ software revealed that approximately 7 %, 11 %, 16 %, and 25.5 % of the surfaces of the untreated W, W_P, S53P4, and SBA2, respectively, were covered with bacterial cells. However, these areas significantly decrease to about 3–4 % for the treated samples (Fig. 11b). To check larger areas of the samples' surfaces using ImageJ software, SEM images with low magnifications (× 2000) were used as explained in detail in Section 2.4.2; Fig. 10c shows the SEM and ImageJ images for S53P4 and its treated counterpart (S53P4_T) as representative of all samples.

This characteristic of HDMSO plasma treatment can be explained based on the results obtained from static contact angle measurements (Fig. 5). According to these results, the hydrophobicity of all samples' surfaces, both inert and bioactive glasses, was significantly increased by coating with HDMSO due to the exposure of CH_3 groups on the top layer of the surfaces, also evidenced by FTIR analysis. The measured water contact angle (WCA) for S53P4_T samples reached over 90°, which, according to previous literature, categorizes them as hydrophobic surfaces [67,68]. The increase in hydrophobicity reduces the contact area between the bacterial suspensions and the samples' surfaces, leading to less bacterial adherence on the surfaces (Fig. 11a) [46].

In summary, the presence of the coating and the exposure of the CH_3

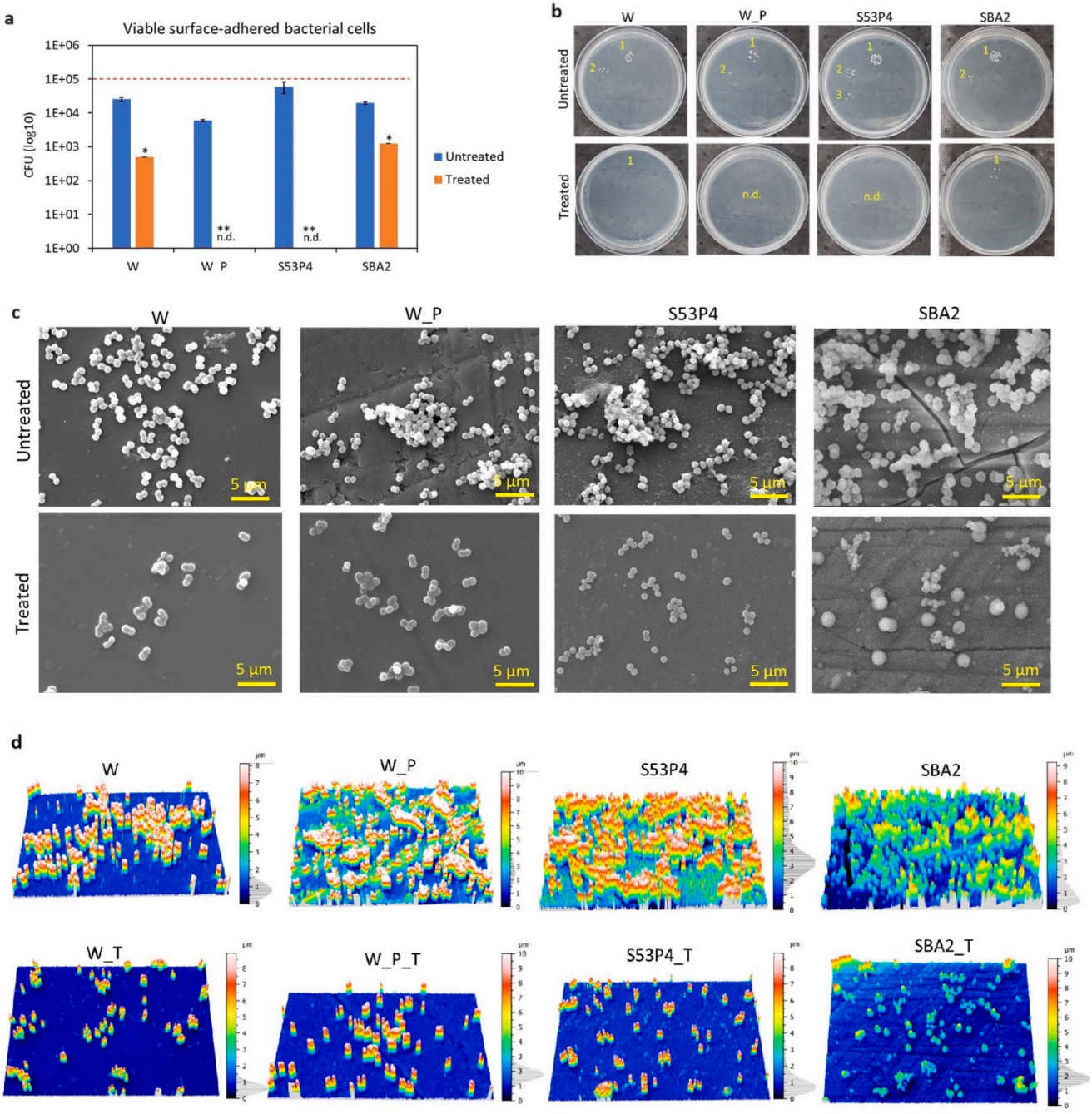

Fig. 10. Antifouling properties of the inert and bioactive glasses by HDMSO plasma treatment. a) Number of viable surface-adhered bacterial cells; the red line indicates the starting number of MDR *S. aureus* (1×10^5 CFU/mL), with * and ** representing p values <0.05 and <0.01, respectively; b) CFU plate images; c) SEM images of surface-adhered bacterial cells, scale bar = 5 µm (× 4000); d) 3D-reconstructed SEM images, SEM images at low magnification (× 2000) used for this analysis.

groups confer an anti-adhesive effect to all the materials investigated. Obtaining even higher contact angles (superhydrophobic surfaces) could further improve the anti-adhesive properties; however, as highlighted by some papers [69], contact angles that are too high can disrupt cell adhesion. The objective of the present work (concerning bioactive glasses) is to obtain anti-adhesive surfaces without inhibiting the bioactivity mechanism and cell adhesion. For this reason, future developments must focus on the evaluation of cytocompatibility.

5. Conclusions

In this work, a successful deposition of HDMSO on both inert and bioactive glasses through a non-thermal atmospheric plasma technique was achieved. The obtained coatings are uniform and impart a good degree of hydrophobicity to the different glass compositions due to the exposure of CH_3 groups. The presence of the coating slightly decreases the bioactivity kinetics of the two investigated glasses, but the precipitation of hydroxyapatite is still observed after 7 days of immersion in SBF.

The antifouling evaluation of HDMSO plasma-treated inert and bioactive glasses showed a significant reduction in the number of viable surface-adhered MDR *S. aureus*, the height of bacterial aggregations and the occupied surface area on the samples' surfaces by bacterial cells compared to the corresponding untreated samples as control. These

a

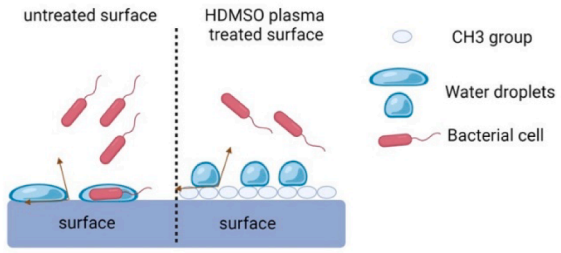

b

Samples	Counted bacterial cells	Total occupied area (μm²)	Occupied Area (%)
W	358	235.211	6.964
W_T	145	131.627	3.897
W_P	512	378.057	11.194
W_P_T	129	127.937	3.788
S53P4	731	541.05	16.02
S53P4_T	176	106.104	3.142
SBA2	586	810.773	25.607
SBA2_T	116	112.157	3.535

c

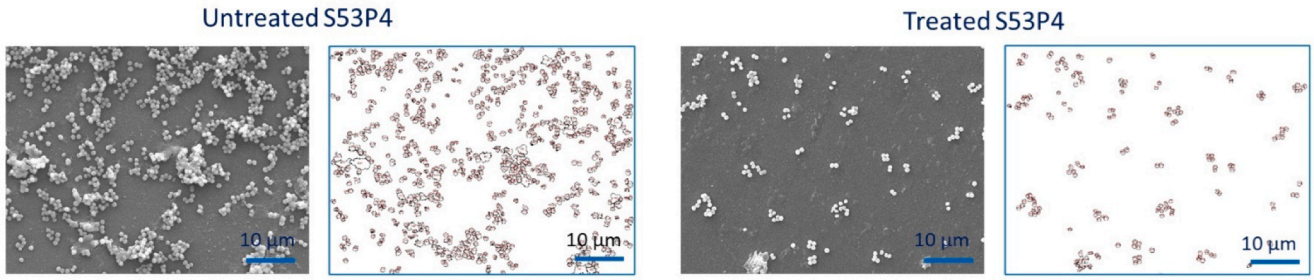

Fig. 11. Effect of surface hydrophobicity on bacterial adherence and evaluation of occupied surface area on samples' surfaces with MDR *S. aureus*. a) Schematic diagram showing bacterial adherence on surfaces with different wettability; b) Values of counted bacterial cells and occupied area on the samples' surfaces with bacteria, using ImageJ software; c) SEM and ImageJ images for S53P4 and treated S53P4 as representatives of all tested samples (scale bar = 10 μm).

reductions were particularly noticeable for treated S53P4 and W_P, which, according to the static water angle, had significantly changed surface wettability after HDMSO plasma treatment. Specifically, for S53P4, the WCA reached over 90°, categorizing it as a hydrophobic surface and leading to the adherence of fewer bacteria on the surface due to the decreased contact areas between bacterial cells and the surface. However, given the hydrophobic nature of the obtained surfaces, cell adhesion will need to be assessed.

Overall, these results showed a high potential of HDMSO plasma treatments to confer anti-adhesive properties to glasses, maintaining, for bioactive glasses, a good bioactivity degree, useful for positive active interaction between the material and the bone tissue.

CRediT authorship contribution statement

Marta Miola: Writing – original draft, Supervision, Resources, Methodology, Investigation, Data curation, Conceptualization. **Kevin Pontillo:** Writing – original draft, Investigation, Formal analysis. **Katiuscia Costabello:** Resources, Methodology, Investigation, Conceptualization. **Manuel Lai:** Resources. **Sara Ferraris:** Writing – original draft, Investigation, Formal analysis. **Ziba Najmi:** Writing – original draft, Investigation, Formal analysis. **Andrea Cochis:** Writing – original draft, Methodology. **Lia Rimondini:** Supervision. **Enrica Vernè:** Supervision, Conceptualization.

Declaration of competing interest

The authors declare that they have no known competing financial interests or personal relationships that could have appeared to influence the work reported in this paper.

Data availability

Data will be made available on request.

References

[1] B. Demirel, M.Erol Taygun, Production of soda lime glass having antibacterial property for industrial applications, Materials. 13 (2020) 4827, https://doi.org/10.3390/ma13214827.
[2] D. Guldiren, S. Aydin, Characterization and antimicrobial properties of soda lime glass prepared by silver/sodium ion exchange, Mater. Sci. Eng. 67 (2016) 144–150, https://doi.org/10.1016/j.msec.2016.04.109.
[3] V. Kisand, M. Visnapuu, M. Rosenberg, D. Danilian, S. Vlassov, M. Kook, S. Lange, R. Pärna, A. Ivask, Antimicrobial activity of commercial photocatalytic SaniTise^{TM} window glass, Catalysts. 12 (2022) 197, https://doi.org/10.3390/catal12020197.
[4] L. Drago, M. Toscano, M. Bottagisio, Recent evidence on bioactive glass antimicrobial and antibiofilm activity: a mini-review, Materials. 11 (2018) 326, https://doi.org/10.3390/ma11020326.
[5] J.A. Otter, S. Yezli, G.L. French, The role played by contaminated surfaces in the transmission of nosocomial pathogens, Infect. Control Hosp. Epidemiol. 32 (2011) 687–699, https://doi.org/10.1086/660363.
[6] J. Hasan, Y. Xu, T. Yarlagadda, M. Schuetz, K. Spann, P.K. Yarlagadda, Antiviral and antibacterial nanostructured surfaces with excellent mechanical properties for hospital applications, ACS. Biomater. Sci. Eng. 6 (2020) 3608–3618, https://doi.org/10.1021/acsbiomaterials.0c00348.
[7] A.A. El-Rashidy, J.A. Roether, L. Harhaus, U. Kneser, A.R. Boccaccini, Regenerating bone with bioactive glass scaffolds: a review of *in vivo* studies in bone defect models, Acta Biomater. 62 (2017) 1–28, https://doi.org/10.1016/j.actbio.2017.08.030.
[8] G. Yi, S.N. Riduan, Y. Yuan, Y. Zhang, Microbicide surface nano-structures, Crit. Rev. Biotechnol. 39 (2019) 964–979, https://doi.org/10.1080/07388551.2019.1641788.
[9] A. Jaggessar, H. Shahali, A. Mathew, P.K.D.V. Yarlagadda, Bio-mimicking nano and micro-structured surface fabrication for antibacterial properties in medical implants, J. Nanobiotechn.. 15 (2017) 1–20, https://doi.org/10.1186/s12951-017-0306-1.
[10] U. Mahanta, M. Khandelwal, A.S. Deshpande, Antimicrobial surfaces: a review of synthetic approaches, applicability and outlook, J. Mater. Sci. 56 (2021) 17915–17941, https://doi.org/10.1007/s10853-021-06404-0.
[11] X.M. Yang, J.W. Hou, Y. Tian, J.Y. Zhao, Q.Q. Sun, S.B. Zhou, Antibacterial surfaces: strategies and applications, Sci. China Technol. Sci. 65 (2022) 1000–1010, https://doi.org/10.1007/s11431-021-1962-x.
[12] K. Vasilev, S.S. Griesser, H.J. Griesser, Antibacterial surfaces and coatings produced by plasma techniques, Plasma Proc. Polym. 8 (2011) 1010–1023, https://doi.org/10.1002/ppap.201100097.
[13] S.S. Latthe, C. Terashima, K. Nakata, A. Fujishima, Superhydrophobic surfaces developed by mimicking hierarchical surface morphology of lotus leaf, Molecules. 19 (2014) 4256–4283, https://doi.org/10.3390/molecules19044256.
[14] G.S. Watson, D.W. Green, L. Schwarzkopf, X. Li, B.W. Cribb, S. Myhra, J.A. Watson, A gecko skin micro/nano structure - A low adhesion, superhydrophobic, anti-

wetting, self-cleaning, biocompatible, antibacterial surface, Acta Biomater. 21 (2015) 109–122, https://doi.org/10.1016/j.actbio.2015.03.007.
[15] E. Verné, M. Miola, C. Vitale Brovarone, M. Cannas, S. Gatti, G. Fucale, G. Maina, A. Massé, S. Di Nunzio, Surface silver-doping of biocompatible glass to induce antibacterial properties. Part I: massive glass, J. Mater. Sci. Mater. Med. 20 (2009) 733–740, https://doi.org/10.1007/s10856-008-3617-9.
[16] M. Lallukka, M. Miola, Z. Najmi, A. Cochis, S. Spriano, L. Rimondini, E. Verné, Cu-doped bioactive glass with enhanced *in vitro* bioactivity and antibacterial properties, Ceram. Int. 50 (2024) 5091–5103, https://doi.org/10.1016/j.ceramint.2023.11.253.
[17] A. Sayed Abdelgeliel, S. Ferraris, A. Cochis, S. Vitalini, M. Iriti, H. Mohammed, A. Kumar, M. Cazzola, W.M. Salem, E. Verné, S. Spriano, L. Rimondini, Surface functionalization of bioactive glasses with polyphenols from padina pavonica algae and in situ reduction of silver ions: physico-chemical characterization and biological response, Coatings 9 (2019) 394, https://doi.org/10.3390/coatings9060394.
[18] M. Miola, E. Bertone, E. Vernè, In situ chemical and physical reduction of copper on bioactive glass surface, Appl. Surf. Sci. 495 (2019) 143559, https://doi.org/10.1016/j.apsusc.2019.143559.
[19] M. Miola, E. Verné, Bioactive and antibacterial glass powders doped with copper by ion-exchange in aqueous solutions, Materials. 9 (2016) 405, https://doi.org/10.3390/ma9060405.
[20] S. Ferraris, M. Miola, A. Cochis, B. Azzimonti, L. Rimondini, E. Prenesti, E. Vernè, In situ reduction of antibacterial silver ions to metallic silver nanoparticles on bioactive glasses functionalized with polyphenols, Appl. Surf. Sci. 396 (2017) 461–470, https://doi.org/10.1016/j.apsusc.2016.10.177.
[21] I. Gonzalo-Juan, F. Xie, M. Becker, D.U. Tulyaganov, E. Ionescu, S. Lauterbach, F. De Angelis Rigotti, A. Fischer, R. Riedel, Synthesis of silver modified bioactive glassy materials with antibacterial properties via facile and low-temperature route, Materials. 13 (2020) 5115, https://doi.org/10.3390/ma13225115.
[22] M. Miola, C. Vitale-Brovarone, C. Mattu, E. Verné, Antibiotic loading on bioactive glasses and glass-ceramics: an approach to surface modification, J. Biomater. Appl. 28 (2013) 308–319, https://doi.org/10.1177/0885328212447665.
[23] K. Zheng, M. Lu, Y. Liu, Q. Chen, N. Taccardi, N. Hüser, A.R. Boccaccini, Monodispersed lysozyme-functionalized bioactive glass nanoparticles with antibacterial and anticancer activities, Biomed. Mater. 11 (2016) 035012, https://doi.org/10.1088/1748-6041/11/3/035012.
[24] S. Shaikh, D. Singh, M. Subramanian, S. Kedia, A.K. Singh, K. Singh, N. Gupta, S. Sinha, Femtosecond laser induced surface modification for prevention of bacterial adhesion on 45S5 bioactive glass, J. Non. Cryst. Solids. 482 (2018) 63–72, https://doi.org/10.1016/j.jnoncrysol.2017.12.019.
[25] Y. Won, K. Schwartzenberg, K.A. Gray, Chemosphere TiO 2 -based transparent coatings create self-cleaning surfaces, Chemosphere 208 (2018) 899–906, https://doi.org/10.1016/j.chemosphere.2018.06.014.
[26] H. Choi, S. Seo, J. Jung, S. Yoon, Water-resistant and antibacterial zinc aluminate films : application of antibacterial thin film capacitors, (2021) 1–8. https://doi.org/10.1021/acsaelm.1c00055.
[27] E.N. Gkana, A.I. Doulgeraki, N.G. Chorianopoulos, Anti-adhesion and anti-biofilm potential of organosilane nanoparticles against foodborne pathogens, 8 (2017) 1–9. https://doi.org/10.3389/fmicb.2017.01295.
[28] D. Marra, I. Perna, G. Pota, G. Vitiello, A. Pezzella, G. Toscano, G. Luciani, S. Caserta, Nanoparticle coatings on glass surfaces to prevent pseudomonas fluorescens AR 11 biofilm formation, Microorganisms. 11 (2023) 621, https://doi.org/10.3390/microorganisms11030621.
[29] Corning S.r.l., World's first antimicrobial cover glass: antimicrobial corning® gorilla® glass https://www.corning.com/gorillaglass/worldwide/en/glass-types/antimicrobial-gorilla-glass.html, 2024 (accessed 14 May 2024).
[30] Corning S.r.l., Antimicrobial corning ® gorilla ® glass product information https://www.corning.com/microsites/csm/gorillaglass/PI_Sheets/CGG_PI_Sheet_Antimicrobia_Gorilla_Glass.pdf, 2014 (accessed 14 May 2024).
[31] A. Nikiforov, C. Ma, A. Choukourov, F. Palumbo, Plasma technology in antimicrobial surface engineering, J. Appl. Phys. 131 (2022) 011102, https://doi.org/10.1063/5.0066724.
[32] M. Guo, F. Meng, G. Li, J. Luo, X. Xia, Effective antibacterial glass fiber membrane prepared by plasma- enhanced chemical grafting, ACS. Omega 4 (2019) 16591–16596, https://doi.org/10.1021/acsomega.9b02403.
[33] C. Tran, M. Yasir, D. Dutta, N. Eswaramoorthy, N. Suchowerska, M. Willcox, D. R. Mckenzie, Single step plasma process for covalent binding of antimicrobial peptides on catheters to suppress bacterial adhesion, ACS. Appl. Bio Mater. 2 (2019) 5216–6028, https://doi.org/10.1021/acsabm.9b00776.
[34] C. García-Bonillo, R. Texido, J. Gilabert-Porres, S. Borros, Plasma-induced nanostructured metallic silver surfaces : study of bacteriophobic effect to avoid bacterial adhesion on medical devices, Heliyon. 8 (2022), https://doi.org/10.1016/j.heliyon.2022.e10842.
[35] V. Mazánková, P. St'ahel, P. Matoušková, A. Brablec, J. Cech, L. Prokeš, V. Buršíková, M. Stupavská, M. Lehocký, K. Ozaltin, P. Humpolícek, D. Trunec, Atmospheric pressure plasma polymerized 2-Ethyl-2-oxazoline based thin films for, Polymers. (Basel) 12 (2020) 1–15, https://doi.org/10.3390/polym12112679.
[36] A. Al-jumaili, K. Bazaka, M.V. Jacob, Retention of antibacterial activity in geranium plasma polymer thin films, Nanomaterials 7 (2017), https://doi.org/10.3390/nano7090270.
[37] K.S. Siow, A. Syahirah, A. Rahman, P. Yuen, B.Y. Majlis, Materials science & engineering c sulfur and nitrogen containing plasma polymers reduces bacterial attachment and growth, Mater. Sci. Eng. C 107 (2020) 110225, https://doi.org/10.1016/j.msec.2019.110225.
[38] A. Kumar, A. AlJumaili, K. Prasad, K. Bazaka, P. Mulvey, J. Warner, M.V. Jacob, Pulse plasma deposition of terpinen4ol: an insight into polymerization mechanism and enhanced antibacterial response of developed thin films, plasma chemistry and plasma processing 40 (2020) 339–355. https://doi.org/10.1007/s11090-019-10045-2.
[39] A. Holmström, A. Meriläinen, J. Hyvönen, A. Nolvi, T. Ylitalo, K. Steffen, R. Björkenheim, G. Strömberg, H.J. Nieminen, I. Kassamakov, J. Pajarinen, L. Hupa, A. Salmi, E. Hæggström, N.C. Lindfors, Evaluation of bone growth around bioactive glass S53P4 by scanning acoustic microscopy co-registered with optical interferometry and elemental analysis, Sci. Rep. 13 (2023) 6646, https://doi.org/10.1038/s41598-023-33454-y.
[40] M. Miola, G. Fucale, G. Maina, E. Verné, Antibacterial and bioactive composite bone cements containing surface silver-doped glass particles Antibacterial and bioactive composite bone cements containing surface silver-doped glass particles, Biomedic. Mater. 10 (2015), https://doi.org/10.1088/1748-6041/10/5/055014.
[41] M. Miola, G. Fucale, G. Maina, E. Verné, Antibacterial and bioactive composite bone cements containing surface silver-doped glass particles Antibacterial and bioactive composite bone cements containing surface silver-doped glass particles, Biomedic. Mater. 10 (2015), https://doi.org/10.1088/1748-6041/10/5/055014.
[42] A. Cochis, J. Barberi, S. Ferraris, M. Miola, L. Rimondini, E. Vernè, S. Yamaguchi, S. Spriano, Competitive surface colonization of antibacterial and bioactive materials doped with strontium and/or silver ions, Nanomaterials 10 (2020) 120, https://doi.org/10.3390/nano10010120.
[43] M. Lallukka, A. Houaoui, M. Miola, S. Miettinen, J. Massera, E. Verné, *In vitro* cytocompatibility of antibacterial silver and copper-doped bioactive glasses, Ceram. Int. 49 (2023) 36044–36055, https://doi.org/10.1016/j.ceramint.2023.08.284.
[44] T. Kokubo, H. Takadama, How useful is SBF in predicting *in vivo* bone bioactivity? Biomaterials 27 (2006) 2907–2915, https://doi.org/10.1016/j.biomaterials.2006.01.017.
[45] M. Gatti, S. Barnini, F. Guarracino, E.M. Parisio, M. Spinicci, B. Viaggi, S. D. Arienzo, S. Forni, A. Galano, F. Gemmi, Orthopaedic implant-associated staphylococcal infections : a critical reappraisal of unmet clinical needs associated with the implementation of the best antibiotic choice, Antibioatics 11 (2022) 406, https://doi.org/10.3390/antibiotics11030406.
[46] E. Sharifikolouei, Z. Najmi, A. Cochis, A.C. Scalia, M. Aliabadi, S. Perero, L. Rimondini, Generation of cytocompatible superhydrophobic Zr – Cu – Ag metallic glass coatings with antifouling properties for medical textiles, Mater. Today Bio 12 (2021), https://doi.org/10.1016/j.mtbio.2021.100148.
[47] V.A. Gobbo, M. Lallukka, F. Gamna, M. Prato, A. Vitale, S. Ferraris, Z. Najmi, A. Cochis, L. Rimondini, J. Massera, S. Spriano, Functionalization of a chemically treated Ti6Al4V-ELI alloy with nisin for antibacterial purposes, Appl. Surf. Sci. 620 (2023) 156820, https://doi.org/10.1016/j.apsusc.2023.156820.
[48] C.P. Stallard, M.M. Iqbal, M.M. Turner, D.P. Dowling, Investigation of the formation mechanism of aligned nano-structured siloxane coatings deposited using an atmospheric plasma jet, Plasma Processes. Polym. 10 (2013) 888–903, https://doi.org/10.1002/ppap.201300056.
[49] M. Mackovic, A. Hoppe, R. Detsch, D. Mohn, W.J. Stark, E. Spiecker, Á.A. R. Boccaccini, Bioactive glass (type 45S5) nanoparticles: *in vitro* reactivity on nanoscale and biocompatibility, J. Nanoparticle Res. 14 (2012), https://doi.org/10.1007/s11051-012-0966-6.
[50] B.R. Barrioni, E. Norris, J.R. Jones, M.D.M. Pereira, The influence of cobalt incorporation and cobalt precursor selection on the structure and bioactivity of sol–gel-derived bioactive glass, J. Solgel. Sci. Technol. 88 (2018) 309–321, https://doi.org/10.1007/s10971-018-4823-7.
[51] P. Navascues, L. Zajíckova, P. Rupper, P. Navascues, M. Buchtelova, D. Hegemann, Polymerization mechanisms of hexamethyldisiloxane in low-pressure plasmas involving complex geometries, Appl. Surf. Sci. 645 (2024), https://doi.org/10.1016/j.apsusc.2023.158824.
[52] S. Shahidi, M. Ghoranneviss, J. Wiener, B. Moazzenchi, H. Mortazavi, Effect of hexamethyldisiloxane (HMDSO)/nitrogen plasma polymerisation on the anti felting and dyeability of wool fabric, Fibres and Textiles in Eastern, Europe 105 (2014) 116–119.
[53] X. Xie, T. de los Arcos, G. Grundmeier, Comparative analysis of hexamethyldisiloxane and hexamethyldisilazane plasma polymer thin films before and after plasma oxidation, Plasma Process. Polym. 19 (2022) 1–14, https://doi.org/10.1002/ppap.202200052.
[54] A.S.M. de Freitas, C.C. Maciel, J.S. Rodrigues, R.P. Ribeiro, A.O. Delgado-Silva, E. C. Rangel, Organosilicon films deposited in low-pressure plasma from hexamethyldisiloxane — a review, Vacuum. 194 (2021) 110556, https://doi.org/10.1016/j.vacuum.2021.110556.
[55] P. Navascués, M. Buchtelová, L. Zajícková, P. Rupper, D. Hegemann, Polymerization mechanisms of hexamethyldisiloxane in low-pressure plasmas involving complex geometries, Appl. Surf. Sci. 645 (2024) 158824, https://doi.org/10.1016/j.apsusc.2023.158824.
[56] M. Jaritz, P. Alizadeh, L. Kleines, R. Dahlmann, S. Wilski, Comparison of HMDSO and HMDSN as precursors for high-barrier plasma-polymerized multilayer coating systems on polyethylene terephthalate films, Plasma Proc. Polym. 18 (2021) 2100018, https://doi.org/10.1002/ppap.202100018.
[57] D. Quéré, Wetting and roughness, Ann. Rev. Mater. Res. 38 (2008) 71–99, https://doi.org/10.1146/annurev.matsci.38.060407.132434.
[58] S. Laurén, Wenzel equation – How roughness is related to wettability? Biolin Scient. (2020). https://www.biolinscientific.com/blog/wenzel-equation-how-roughness-is-related-to-wettability (accessed May 14, 2024).
[59] C. Ma, A. Nikiforov, D. Hegemann, N. De Geyter, R. Morent, K. (Ken) Ostrikov, Plasma-controlled surface wettability: recent advances and future applications, Int.

Mater. Rev. 68 (2023) 82–119, https://doi.org/10.1080/09506608.2022.2047420.
[60] M. Kosmulski, Journal of Colloid and Interface Science pH-dependent surface charging and points of zero charge . IV . Update and new approach, J. Colloid. Interface Sci. 337 (2009) 439–448, https://doi.org/10.1016/j.jcis.2009.04.072.
[61] M.J. Owen, P.R. Dvornic, Silicone Surface Science, Springer, Netherlands, Dordrecht, 2012, https://doi.org/10.1007/978-94-007-3876-8.
[62] S. Ferraris, A. Nommeots-nomm, S. Spriano, E. Vernè, J. Massera, Applied surface science surface reactivity and silanization ability of borosilicate and Mg-Sr-based bioactive glasses, Appl. Surf. Sci. 475 (2019) 43–55, https://doi.org/10.1016/j.apsusc.2018.12.218.
[63] S. Ferraris, S. Yamaguchi, N. Barbani, M. Cazzola, C. Cristallini, M. Miola, E. Vernè, S. Spriano, Bioactive materials: *in vitro* investigation of different mechanisms of hydroxyapatite precipitation, Acta Biomater. (2019) 0–38, https://doi.org/10.1016/j.actbio.2019.11.024.
[64] T. Luxbacher, The ZETA guide, principles of the streaming potential technique. Anton Paar GmbH, 1st Edition, 2014, pp. 1–136.
[65] M. Ribeiro, F.J. Monteiro, M.P. Ferraz, Infection of orthopedic implants with emphasis on bacterial adhesion process and techniques used in studying bacterial-material interactions Infection of orthopedic implants with emphasis on bacterial adhesion process and techniques used in studying bacte, Biomatter. 2 (2012) 176–194, https://doi.org/10.4161/biom.22905.
[66] D.G. Kennedy, A.M. O'Mahony, E.P. Culligan, C.M. O'Driscoll, K.B. Ryan, Strategies to mitigate and treat orthopaedic device-associated infections, Antibiotics 11 (2022) 1822, https://doi.org/10.3390/antibiotics11121822.
[67] K. Law, Definitions for hydrophilicity, hydrophobicity, and superhydrophobicity: getting the basics right, J.f Physic. Chem. Lett. 5 (2014) 686–688, https://doi.org/10.1021/jz402762h.
[68] C. Corsaro, D. Mallamace, G. Neri, E. Fazio, Hydrophilicity and hydrophobicity: key aspects for biomedical and technological purposes, Physica. A 580 (2021) 126189, https://doi.org/10.1016/j.physa.2021.126189.
[69] J. Wei, M. Yoshinari, S. Takemoto, M. Hattori, E. Kawada, B. Liu, Y. Oda, Adhesion of mouse fibroblasts on hexamethyldisiloxane surfaces with wide range of wettability, J. Biomed. Mater. Res. B Appl. Biomater. 81B (2007) 66–75, https://doi.org/10.1002/jbm.b.30638.